Optics Letters

3D transient wind camera incorporating 20 × 5 time-division multiplexing MIMO Doppler lidar

Jinlong Yuan,[1,2] Shuo Zhang,[2] Jiadong Hu,[2,3] Jiawei Qiu,[2] Kenan Wu,[4] Wei Tian,[1] and Haiyun Xia[1,2,3,5,*]

[1]State Key Laboratory of Precision Spectroscopy, East China Normal University, Shanghai 200241, China
[2]State Key Laboratory of Climate System Prediction and Risk Management, NUIST, Nanjing 210044, China
[3]Key Laboratory of Intelligent Support Technology for Complex Environments, Ministry of Education, Nanjing University of Information Science and Technology, Nanjing 210044, China
[4]School of Information Engineering, Huangshan University, Huangshan 245041, China
[5]Institute of Lidar Technology, GuangZai Co., Ltd., Hangzhou 310005, China
*hsia@ustc.edu.cn

Received 12 August 2026; revised 30 September 2026; accepted 8 October 2026; posted 9 October 2026; published 12 November 2026

To capture rapidly evolving three-dimensional atmospheric flows, a stereoscopic wind camera incorporating 20 × 5 time-division-multiplexing MIMO Doppler lidar is proposed and experimentally validated. Evolving from a planar wind camera, the system combines a 10 × 10 focal-point array in a single-aperture multichannel telecentric telescope and 20 integrated laser–receiver pairs. Each pair sequentially measures five channels, while parallel data acquisition and transmission enable 100-channel volumetric sampling within a 1 s cycle. The system achieves a 30° field of view and a maximum detection range of 2.5 km. Rapid volumetric sampling of line-of-sight velocities reveals wind-field evolution, providing a temporally consistent set of observations for three-dimensional variational wind vector retrieval. This architecture enables high-refresh-rate observations of transient flows, with promising applications in aviation safety, meteorology, and wind engineering. © 2026 Optica Publishing Group. All rights, including for text and data mining (TDM), Artificial Intelligence (AI) training, and similar technologies, are reserved.

https://doi.org/10.1364/OL.614241

Three-dimensional (3D) high-dynamic flows are ubiquitous in practical scenarios, including aircraft vortices, building wakes, turbine wakes, and gust fronts, which are crucial for aviation safety, meteorological research, and wind engineering [1,2]. Resolving these structures requires wide-range coverage, dense 3D sampling, and high spatiotemporal resolution. Conventional in-situ anemometers only provide single-point measurements. Particle image velocimetry (PIV) offers high spatial resolution but requires tracer seeding and controlled illumination, limiting its use to meter-scale laboratory and wind-tunnel measurements. These limitations motivate a remote-sensing instrument that combines extensive spatial coverage, 3D sampling, and high spatiotemporal resolution.

Coherent Doppler wind lidar (CDWL) has been widely used for atmospheric wind sensing because of its high spatiotemporal resolution and flexible scanning capability [3–5]. Multielevation plan-position-indicator (PPI) scans can retrieve 3D wind vectors [6,7]. However, traditional sequential scanning mode consumes a long time to complete 3D spatial sampling. This leads to inevitable time-lag effects, which make it difficult to capture rapidly changing 3D turbulent structures, as spatial scanning density and time consumption are mutually constrained. It introduces significant errors in wind field retrieval, especially for highly variable flows.

To mitigate time-lag errors, a few multichannel lidar systems have been reported for wind profile detection [8,9], but most adopt beam-switching or multitelescope configurations, with limited spatial coverage and increased system complexity. We previously developed a 10-channel planar wind camera that enabled synchronous two-dimensional horizontal wind-field imaging through parallel multibeam detection, thereby eliminating errors caused by wind-field evolution during scanning [10]. Nevertheless, this planar system is only capable of horizontal wind-field imaging and cannot capture vertical airflow components, failing to meet the demand for 3D wind-field detection in complex scenarios.

To address these limitations, we extend the previous 10-channel planar system to a 100-channel stereoscopic wind camera. By using a 20 × 5 matrix of transmitting and receiving channels, the system enables synchronous 3D wind-field sampling, transforming planar imaging into volumetric sensing.

The system incorporates a 20 × 5 time-division-multiplexing (TDM) multiple-input multiple-output (MIMO) Doppler lidar. The layout of the optical transceiver system is shown in Figs. 1(a) and 1(b). The laser and acquisition array contains 20 pairs of lasers and integrated receivers. The laser module is shown in Fig. 1(c). For each laser module, a continuous-wave laser (CWL) at 1550 nm is split into two parts. One portion of the CWL laser serves as local oscillator light. The remaining portion is frequency-shifted by 80 MHz via an acousto-optic modulator (AOM). The frequency-shifted beam is then amplified by an erbium-doped fiber amplifier (EDFA). The transmitted laser achieves 5-channel beam switching via a high-speed optical switch (OS) and is connected to the 20 × 5 focal point array on the telescope, as shown in Fig. 1(b). The backscattered echo signal from the atmosphere is collected by the same telescope

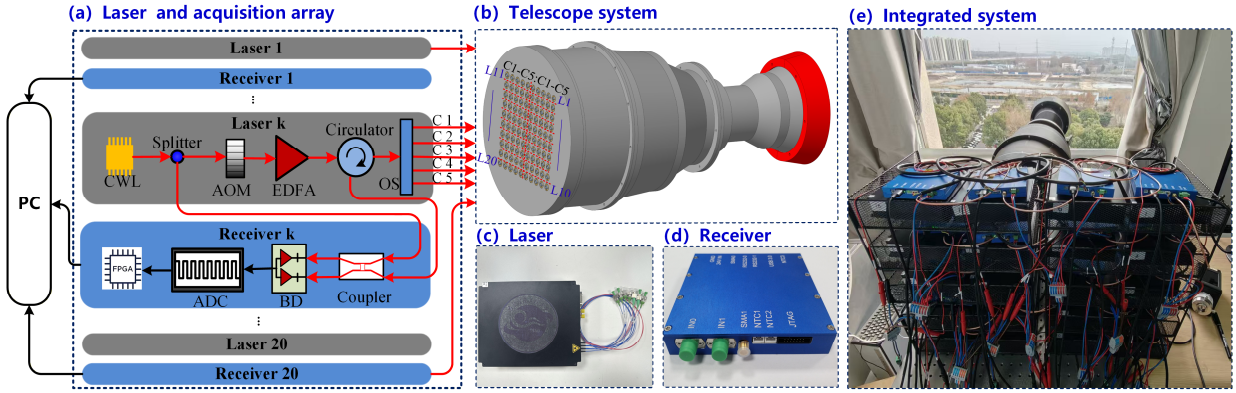


Fig. 1. Diagram of the stereoscopic wind camera. (a) System layout of the laser and acquisition array. ADC, analog-to-digital converter; AOM, acoustic–optic modulator; BD, balanced photodetector; CWL, continuous-wave laser; EDFA, erbium-doped fiber amplifier; OS, optical switch; PC, personal computer. (b) The telescope system. (c) The integrated laser module. (d) The integrated receiver. (e) The integrated system used in the experiment.

and mixed with the LO light to generate beat signals. Subsequently, the beat-frequency light signal is fed into the balanced photodetector (BD).

The integrated receiver has dimensions of 110 mm × 103 mm × 20 mm with a power of 25 W, as shown in Fig. 1(d). Each integrated receiver contains four modules: a coupler, an InGaAs PIN diode-based BD, a high-speed analog-to-digital converter (ADC), and an FPGA chip, which sequentially implement signal mixing, photoelectric conversion, time-domain signal acquisition, and fast Fourier transform (FFT) computation. The power of the local oscillator on each BD is optimized to 0.55 mW. The common-mode rejection ratio (CMRR), responsivity, and bandwidth of the BD are >25 dB, >0.8 mA/mW, and 200 MHz, respectively.

Figure 1(b) is a diagram of the single-aperture multichannel telescope, which adopts a double-Gaussian symmetric and image-side telecentric design. The detailed design is described in the previous work [10]. Notably, the focal point array is upgraded from 1 × 10 to 20 × 5. The focal points form a uniform square array centered on the optical axis, with 20.8 mm spacing between adjacent focal points. The diagonal length of the square is 264.74 mm, corresponding to a field of view (FOV) of 30°. The focal point array is uniformly partitioned into 20 1 × 5 subarrays, with each subarray assigned to the 5 laser (C1 to C5) output channels of one laser module. Each laser module sequentially switches from channel 1 to channel 5 in a periodic manner from left to right.

Each integrated receiver is an independent operation module that finishes the data acquisition, FFT processing, and uploading to the computer over five channels sequentially in 1 s. Figure 2 shows the parallel data acquisition and transmission logic of a single receiver. The upper sequence shows that the system performs time-domain signal acquisition and FFT processing on each channel sequentially. Each channel (e.g., Channel N-1) requires 0.18 s for acquisition and real-time FFT processing, followed by a 0.02 s switching period to the next channel (Channel N), resulting in a fixed cycle of 0.2 s per channel. Meanwhile, the lower sequence demonstrates that while the system is processing Channel N-1, it simultaneously uploads the data from the earlier-completed Channel N-2 to the PC via USB. This parallel design enables the overlapping of acquisition/processing and data upload tasks, which not only ensures stable timing but also

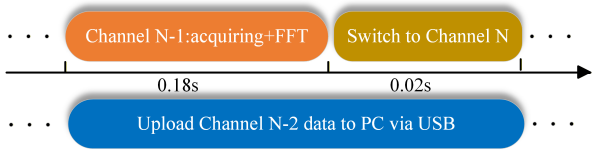


Fig. 2. Parallel data acquisition and transmission logic of a receiver.

significantly improves the overall efficiency of the system. Notably, a common trigger aligns the switching and acquisition of the 20 laser–receiver pairs. The narrow line-of-sight beam divergence (44 μrad) guarantees no spatial overlap between adjacent channels, and the optical switches provide an inter-port isolation of 50 dB. All these designs make the inter-channel crosstalk negligible.

The key parameters of the stereoscopic wind camera are summarized in Table 1. The pulse duration and pulse energy of the laser are 200 ns and 10 μJ, respectively. The spatial and temporal resolutions of each beam are 30 m and 0.2 s, respectively. With 20 laser–receiver modules operating in parallel and each sequentially addressing five channels, the 20 × 5 TDM architecture completes a 100-channel volumetric acquisition in 1 s without mechanical scanning. Compared with a fully parallel 100-module design, it reduces the module count and associated cost, power consumption, and integration complexity, while introducing a 0.8 s offset between the first and last time slots. Higher laser pulse energy could shorten the accumulation time and increase the volumetric frame rate.

The experiment was carried out at the campus of the Nanjing University of Information Science and Technology (32°12′22″N, 118°42′17″E) on January 11, 2026. The system is installed on the 9th floor (altitude of 30 m) of a building, pointing outward through a window, as shown in Fig. 1(e).

Figure 3(a) presents the 3D line-of-sight (LOS) speed slices for a typical wind field case using a stereoscopic wind camera, where each scanning slice consists of 100 grid points. The maximum detection range reaches 2.5 km, where the measured carrier-to-noise ratio (CNR) is above −20 dB [10]. The observation data show a typical fan-shaped scanning layout along the horizontal distance, with obvious spatial discreteness and local fluctuations.

Table 1. Key Parameters of a Stereoscopic Wind Camera

Module	Parameter	Value
Telescope	Diagonal field of view	30°
	Beam divergence	44 μrad
	Telescope Diameter	125 mm
Laser	Wavelength	1550 nm
	Pulse duration	200 ns
	Pulse energy	10 μJ
	Linewidth	200 kHz
	Repetition frequency	20 kHz
Receiver	Temporal resolution	0.2 s
	Spatial resolution	30 m
	Blind zone	30 m
	Sample rate	500 MS/s

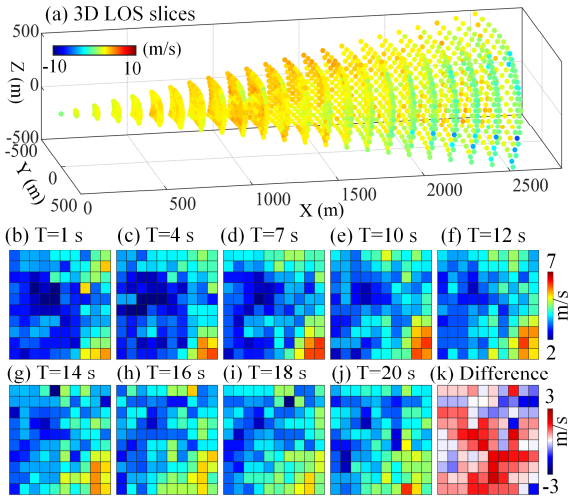


Fig. 3. (a) The 3D LOS slices for a typical wind field. (b)–(j) At a range of R = 300 m, consecutive typical stereoscopic LOS in cross-section snapshots, covering an area of 110 m × 110 m. (k) Absolute LOS velocity difference between the first and last frames of the 20 s sequence.

Each channel takes 0.2 s, and the 20 parallel receiver modules complete a 100-channel volumetric acquisition in 1 s. In contrast, a conventional mechanically scanning wind lidar would require at least 20 s to sample the same volume, corresponding to a 20-fold improvement in volumetric sampling rate. Figures 3(b)–3(j) show consecutive typical stereoscopic LOS in cross-section snapshots from T = 1 s to T = 20 s. At a range of R = 300 m, corresponding range gate of 11, the wind camera can generate a radial wind field composed of 100 grid points, covering an area of 110 m × 110 m. The negative radial speed indicates radial wind speed approaching, and vice versa. The spatial inhomogeneity and dynamic temporal changes of the wind field are clearly visible. However, for a traditional scanning lidar, only a single image can be acquired during this 20 s period, leading to a serious loss of the spatiotemporal variation features of the wind field.

Figure 3(k) shows the absolute line-of-sight velocity difference at each valid grid point between the first and last frames of the 20 s observation sequence. Although the background wind speed is less than 6 m/s, the spatial mean and maximum differences reach 0.8 m/s and 2.4 m/s, respectively. These changes reveal temporal evolution of the wind field and could introduce inconsistencies into 3D wind retrieval when observations are acquired sequentially over a comparable period, especially under highly variable conditions.

The 3D wind field is retrieved from a single 1 s volumetric acquisition of the stereoscopic wind camera. The three-dimensional variational (3DVAR) method is adopted [11], with the objective function J defined as:

$$
\begin{aligned}
J &= J_B + J_r + J_C + J_p \\
J_B &= \sum_{i,j,k} \left[W_{uB} \left(u - u^B\right)^2 + W_{vB} \left(v - v^B\right)^2 + W_{wB} \left(w - w^B\right)^2 \right] \\
J_r &= \frac{1}{2} \sum_{i,j,k} W_r \left(\frac{xu + yv + zw}{r} - v_r^{obs} \right)^2 \\
J_C &= \frac{1}{2} \sum_{i,j,k} W_C \left(\frac{\partial \bar{\rho} u}{\partial x} + \frac{\partial \bar{\rho} v}{\partial y} + \frac{\partial \bar{\rho} w}{\partial z} \right)^2 \\
J_p &= \frac{1}{2} \sum_{i,j,k} \left[W_{pD} (\Delta x)^2 \left(\frac{\partial u}{\partial x} + \frac{\partial v}{\partial y} \right)^2 + W_{pV} (\Delta x)^2 \left(\frac{\partial v}{\partial x} - \frac{\partial u}{\partial y} \right)^2 \right. \\
&\quad \left. + W_{pw} (\Delta x)^4 \left(\nabla^2 w \right)^2 \right]
\end{aligned}
\tag{1}
$$

where J_B is the background term. u, v, and w are the 3 D wind field components to be retrieved. u^B,v^Bandw^B are the background velocities. Setting $J_B = 0$ and $J_p = 0$, the background velocities are obtained via a second-order Legendre polynomial expansion. In the radial observation constraint term J_r, r is the radial distance from the lidar, and x, y, z are the spatial coordinates in the Cartesian coordinate system with the lidar as the origin. In the mass conservation term J_C, $\bar{\rho}$ is the mean air density that varies only with height. In the spatial smoothing term J_p, ∇^2 denotes the Laplacian operator, and Δx is the grid spacing. The weight coefficients in each term are given according to error estimation: $W_{uB} = W_{vB} = W_{wB} = 1.0$, $W_r = 2.0$, $W_C = 1.0 \times 10^5$, $W_{pD} = 10.0$, $W_{pV} = 4.0$, $W_{pw} = 1.0$. These values are empirically chosen to ensure that each constraint term has an appropriate magnitude.

The short acquisition window within 1 s allows the observed wind field to be approximated as quasi-stationary, which is more consistent with the frozen-flow assumption used in the 3DVAR retrieval. Figure 4 shows three successive LOS velocity fields and the corresponding 3D wind fields retrieved by the 3DVAR method at approximately 1 min intervals. The sequence shows that the stereoscopic wind camera can track the temporal evolution of volumetric wind structures over kilometer-scale ranges. A pronounced high-speed airflow region appears at approximately 500 m from the lidar, where the wind-speed magnitude reaches about 6 m/s. Its motion is consistent with the direction of the retrieved wind vectors. The retrieved fields exhibit coherent 3D flow patterns while preserving local velocity variations, indicating that the transient volumetric acquisition provides suitable observations for quasi-stationary 3DVAR retrieval at each time instant. Rapid volumetric sampling can mitigate the time-lag-induced artifacts inherent to sequential scanning.

In summary, this study develops a 100-channel stereoscopic wind camera, enabling high-refresh-rate 3D wind imaging, based on the highly integrated and modularized design of the laser, receiver, and telescope. With 10 μJ energy per channel, a 1 Hz frame rate, and a 2.5 km detection range, it is 20 times

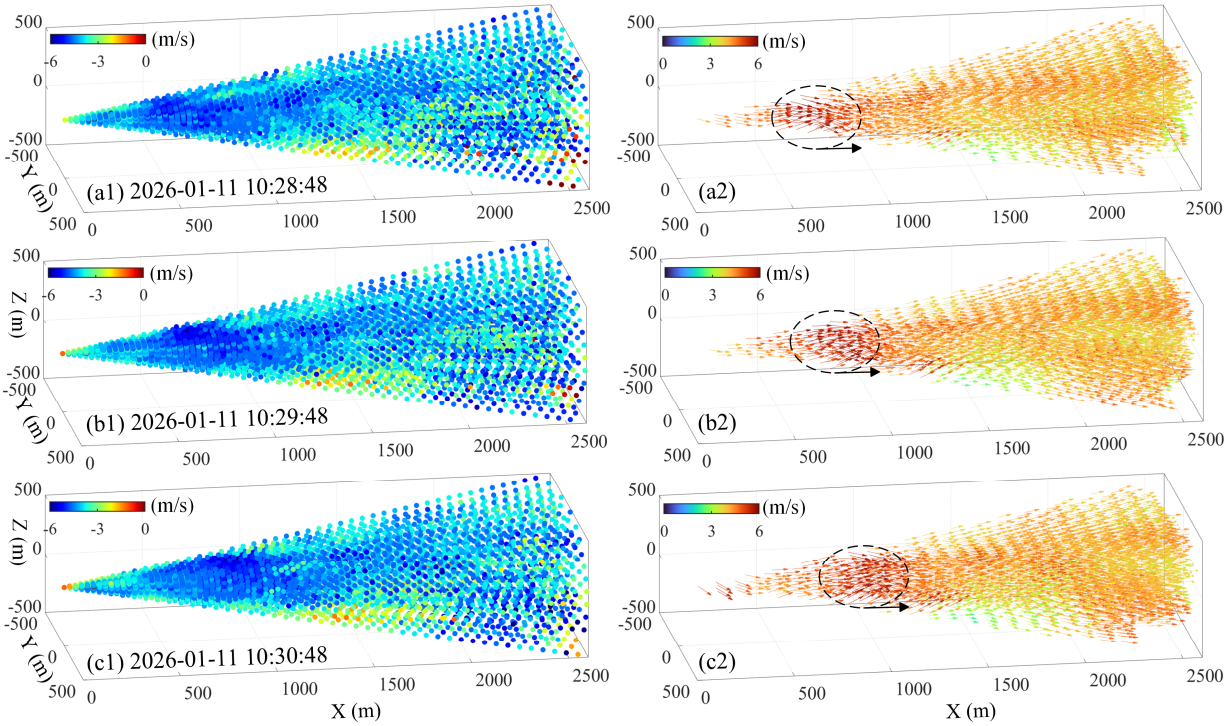


Fig. 4. Temporal evolution of LOS velocity fields and 3D wind vector retrieved by the 3DVAR method. (a1)–(c1) Measured LOS velocity fields at 10:28:48, 10:29:48, and 10:30:48 on January 11, 2026. (a2)–(c2) Corresponding 3D wind-vector fields. Colors represent velocity magnitude, arrows denote wind direction, and dashed circles highlight the evolving high-speed airflow region.

faster than traditional mechanical scanning CDWL. Thus, the system can mitigate errors induced by time-lag effects. The rapid multichannel observation mode of the stereoscopic wind camera, cooperating with the 3DVAR retrieval framework, can effectively overcome the incompleteness of traditional scanning observations and achieve high-quality reconstruction of the three-dimensional wind field with high reliability. This work provides a reliable solution for 3D wind monitoring in aviation, meteorology, and wind energy, overcoming traditional scanning limitations. However, the accuracy of the retrieved 3D wind components remains to be independently validated. Future work will focus on all-weather performance evaluation, improving spatial resolution, and validation against synchronized measurements from a network of Doppler wind lidars observing an overlapping volume.

Funding. National Natural Science Foundation of China (42405137); Key Laboratory of Intelligent Support Technology for Complex Environments, Ministry of Education, NUIST (A1202401); Natural Science Foundation of Jiangsu Province (BK20230434).

Disclosures. The authors declare no conflicts of interest.

Data availability. Data underlying the results presented in this paper are not publicly available at this time but may be obtained from the authors upon reasonable request.

REFERENCES

1. J. Yuan, H. Xia, T. Wei, *et al.*, Opt. Express **28**, 37406 (2020).
2. J. Zhang and X. Zhao, Trans. Appl. Energy **300**, 117390 (2021).
3. Y. Zhang, J. Yuan, Y. Wu, *et al.*, Phys. Rev. Fluids **8**, L022701 (2023).
4. H. Xia, Y. Chen, J. Yuan, *et al.*, Remote Sens. **16**, 924 (2024).
5. S. Wu, X. Zhai, and B. Liu, Opt. Express **27**, 1142 (2019).
6. H. Gao, J. Zhou, P. Chan, *et al.*, IEEE Trans. Geosci. Remote Sens. **60**, 4107012 (2022).
7. L. Huang, H. Gao, P. Chan, *et al.*, IEEE Trans. Geosci. Remote Sens. **64**, 5700216 (2026).
8. H. Tsuji, N. Kotake, S. Kameyama, *et al.*, Opt. Lett. **49**, 2890 (2024).
9. N. Kotake, H. Sakamaki, M. Imaki, *et al.*, Opt. Express **30**, 20038 (2022).
10. J. Yuan, J. Qiu, J. Hu, *et al.*, Opt. Lett. **50**, 5458 (2025).
11. C. Qiu, J. A. Shao, S. Liu, *et al.*, Meteorol. Atmos. Phys. **91**, 1 (2006).